5
Numerical Examples

In this final chapter, we start by illustrating some known results in the theory and then proceed to give a few novel examples.

All examples consider the equation

$$F(u) = -\Delta u - f(u) = g, \tag{5-1}$$

with Dirichlet boundary conditions on the rectangle $\Omega = [0,1] \times [0,2]$. Here,

$$\lambda_1 = \frac{5}{4}\pi^2 \approx 12.34, \quad \lambda_2 = 2\pi^2 \approx 19.74, \quad \lambda_3 = \frac{17}{4}\pi^2 \approx 41.95.$$

Recall that solving (5-1) boils down to performing two steps. First, we move along the space of fibers to identify a point in the fiber α_g. Then we move along this fiber to obtain, in principle, all solutions of the equation.

In the first example, described in Section 5.1, we choose a right-hand side g and compute an element in the fiber α_g.

The subsequent examples, in Section 5.2, correspond to the second step in the algorithm. We suppose that a fiber has been identified and move along the fiber. We first consider scenarios where the fiber is one dimensional.

1. $J = \emptyset$, in the spirit of Hammerstein and Dolph.

2. A typical fiber in the Ambrosetti-Prodi case ($J = \{1\}$ and f convex), which is the α_g obtained in the previous subsection. In particular, we find the solutions of 5-1.

3. Non convex f with $J = \{1\}$.

4. $J = \{2\}$, with convex and non convex f.

In Section 5.3, we conclude with a case in which $J = \{1, 2\}$, for which we present four solutions for a particular g.

The convex nonlinearities $f(x)$ are constructed as follows. We choose constants α and β so that $f'(x) = \alpha \arctan(x) + \beta$ has prescribed asymptotic behavior.

5.1
Moving Horizontally

The first example is a genuine Ambrosetti-Prodi situation:

$$\text{Ran}(f') = \left(\frac{3\lambda_1 - \lambda_2}{2}, \frac{\lambda_1 + \lambda_2}{2} \right) > 0.$$

The right-hand side is chosen to resemble a very negative multiple of the ground state, $g(x) = -100x(x-1)y(y-2)$. We take as initial guess the zero function, $u_0(x) \equiv 0$.

Usually one or two iterations of the horizontal step lead to an error which can only decrease by choosing a finer mesh. An m-triangulation $\mathcal{T}_\Updownarrow$ is the one obtained by splitting $[0,1]$ and $[0,2]$ each in 2^m equal intervals — on the right of Figure A.1, we have a 2-triangulation.

We present the normalized projected errors for triangulations with $m = 3, 4, 5$ and 6: for an approximation u_n, we show $e_n = \frac{||P_{-1}\xi_n||}{||Q_{-1}\xi_n||}$, where $\xi_n = g - F(u_n)$ and the norms are in L^2.

m	e_0	e_1	e_2
3	.03369	.01689	.01688
4	.01635	.00217	.00217
5	.00830	.00028	.00028
6	.00417	.00003	.00003

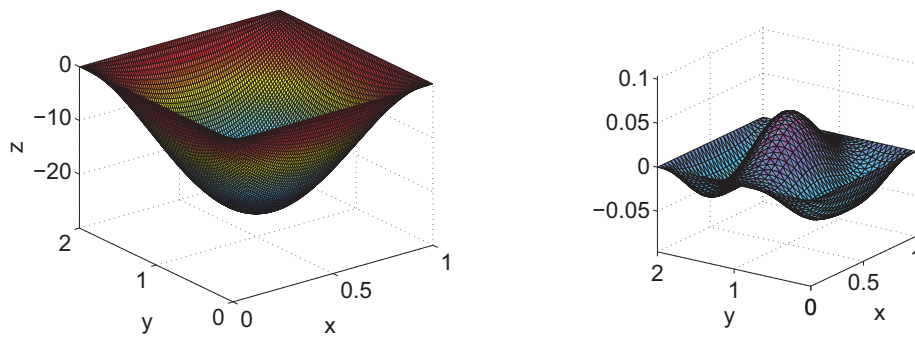In Figure 5.1 we show g and the function u_3.

Figure 5.1: A right-hand side and a function on its fiber

5.2
Moving along a fiber

Unless otherwise stated, we consider fibers through the point

$$u_0(x) = -50\,\varphi_1(x) + 10\,\varphi_2(x),$$

and the vertical subspace is $V_1 = V_{-1} = \mathrm{Span}\{\varphi_1\}$ (we use H^1-normalized eigenfunctions).

5.2.1
The Case $J = \emptyset$

Let us start with the simplest of cases, namely by considering linear functions f, whose derivatives are not equal to eigenvalues of $-\Delta_{Dir}$. In this case, by the linear theory, there is exactly one solution for each right-hand side g. Figure 5.2 is the graph of f': in this case, it lies always below the first
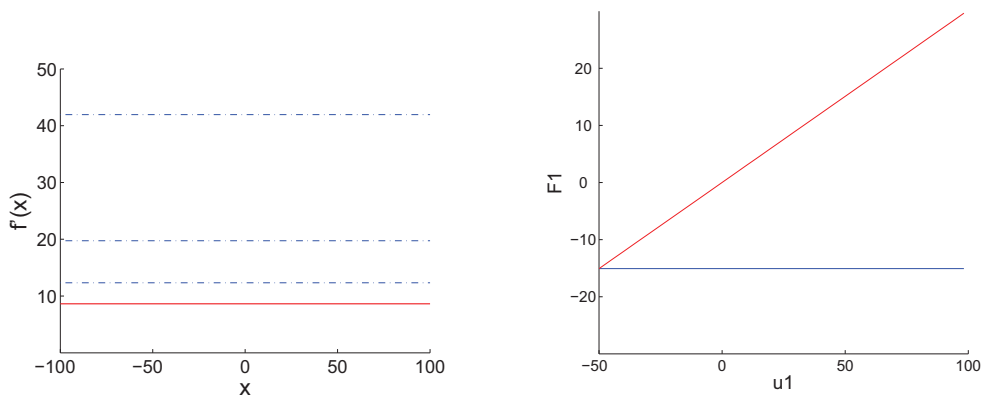
Figure 5.2: $f' < \lambda_1 - \epsilon$
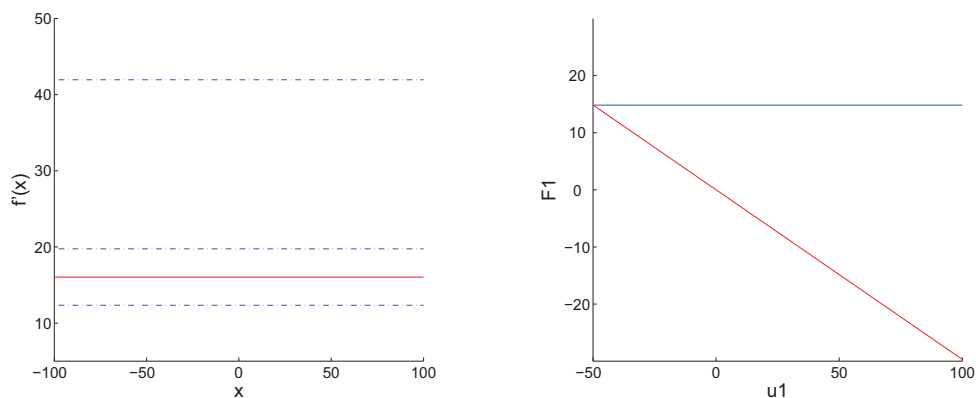
Figure 5.3: $\lambda_1 + \epsilon < f' < \lambda_2 - \epsilon$

eigenvalue. The eigenvalues are marked as dotted lines. The line on the right is

the graph of an increasing function, representing the fact that as we move up along the fiber $u_1 = u_0 + t\varphi_1$, the corresponding point in the range $F_1 = F(u_1)$ also moves up. Similarly, in Figure 5.3, the derivative of f lies strictly between λ_1 and the second eigenvalue. In this case, moving up in the fiber, corresponds to moving down in the range.

We now consider the height variation with respect to the second eigenvector. We set the vertical subspaces $V_1 = V_{-1} = \mathrm{Span}\{\varphi_2\}$ and consider the fiber through

$$u_0(x) = -50\,\varphi_2(x) + 10\,\varphi_1(x).$$

There is a substantial difference between both cases: While on the left of Figure 5.4, we see the same picture as in Figure 5.3. Yet on its right we have an *increasing* line. All is still well, since we are now projecting in φ_2. What we still see is the up-down behavior in the image as we go from being below λ_2 to being above it, as Figure 5.5 confirms.
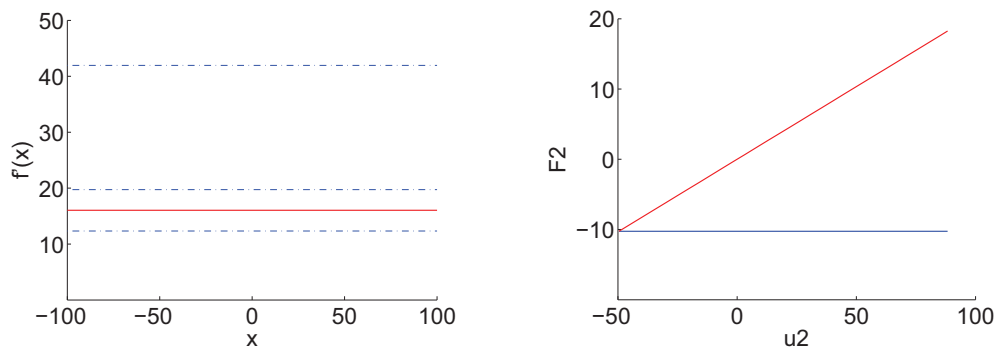

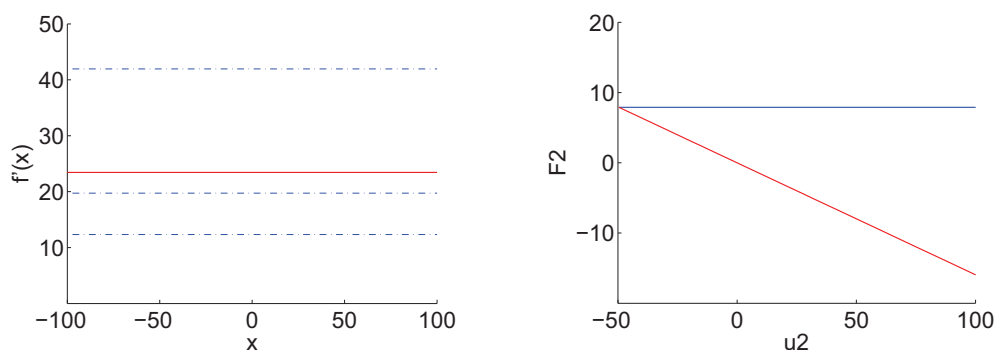Figure 5.4: $\lambda_1 + \epsilon < f' < \lambda_2 - \epsilon$

Figure 5.5: $\lambda_2 + \epsilon < f' < \lambda_3 - \epsilon$

5.2.2
The Ambrosetti-Prodi Case

We now return to the example of Section 5.1. Here we are exactly in the case considered by Ambrosetti and Prodi, of an increasing f' interacting only with the first eigenvalue. A naïve analogy with Figures 5.2 and 5.3 suggests that we start by going up in the range as we move up in the fiber, until we reach a turning point, starting at which we only go downward. This is exactly
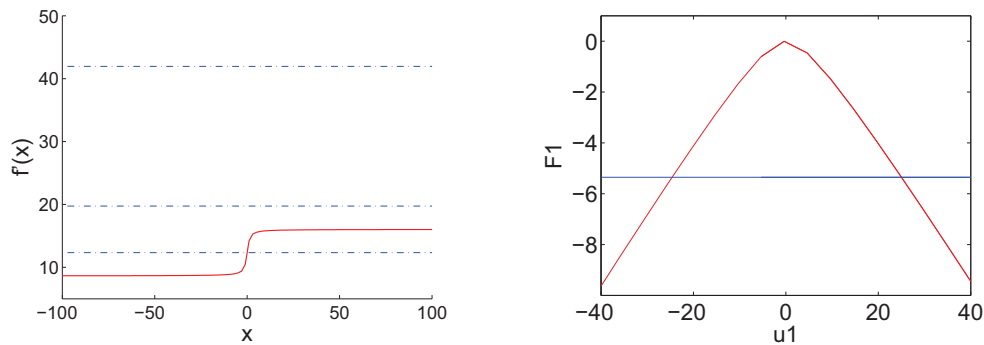

Figure 5.6: $\overline{\operatorname{Ran} f'} \cap \sigma(-\Delta) = \{\lambda_1\}$

what we see in Figure 5.6.

As predicted by the theory, we see that the horizontal line corresponding to the height of the right-hand side $g := F(u_0)$ is crossed twice, indicating that g has two preimages in the fiber, which we present in Figure 5.7.
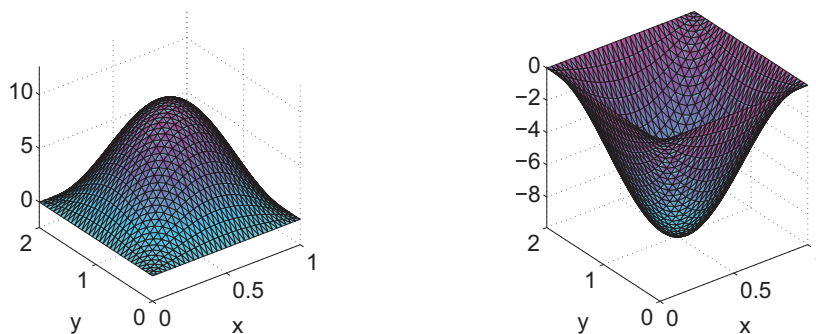
Figure 5.7: Ambrosetti-Prodi Solutions

We combined the correcting algorithm described in Section 4.1.1 with regula falsi.
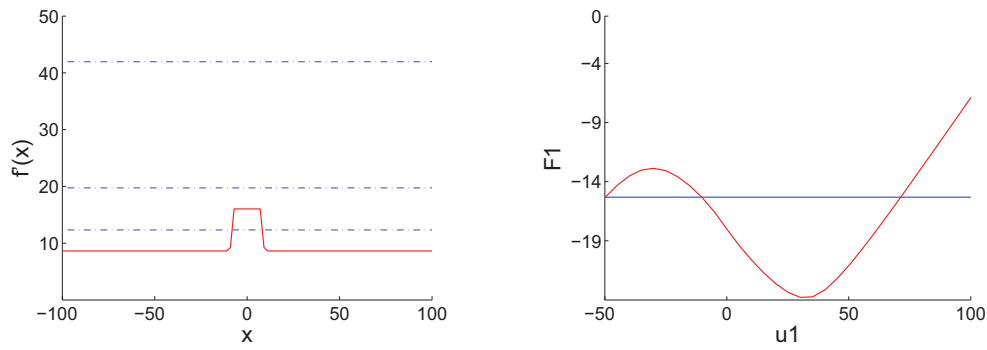
Figure 5.8: Non-convex f

5.2.3
A Non-convex Nonlinearity with $J = \{1\}$

Things get more interesting if we go beyond the Ambrosetti-Prodi case and relax the condition that f be convex. In Figure 5.8 we analyze the situation in which we still interact only with λ_1, but alternating between the behaviors seen in Figures 5.2 and 5.3. Now we have three distinct solutions, $\eta_1 = -50\,\varphi_1 + 10\,\varphi_2$, η_2 and η_3. We chose $g = F(\eta_1)$. These solutions are displayed in Figure 5.9.
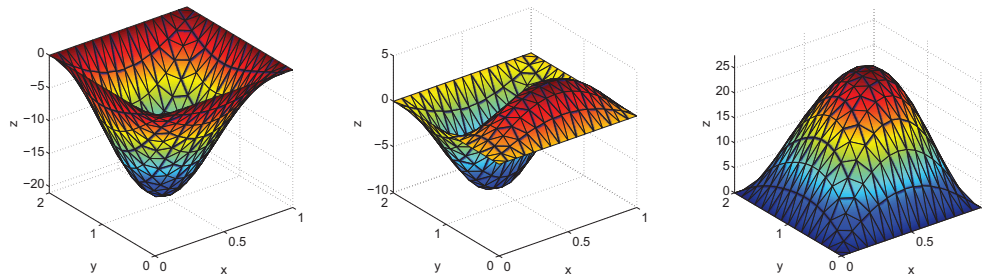
Figure 5.9: Solutions of non-convex case

The sequence in Figure 5.10 shows that the action of F on fibers is *not* homogeneous. The plots are for fibers α_{g_i} with $g_i = F(-50\varphi_1 + c_i\varphi_2)$, where $c_1 = 10$ (same as Fig. 5.8), $c_2 = 45$ and $c_3 = 100$.
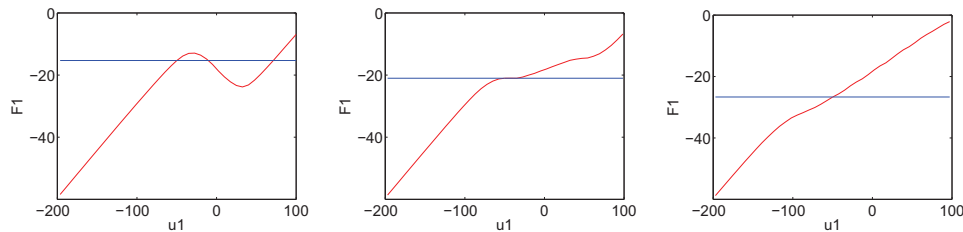

Figure 5.10: Fibers Getting Mapped Non-uniformly

5.2.4
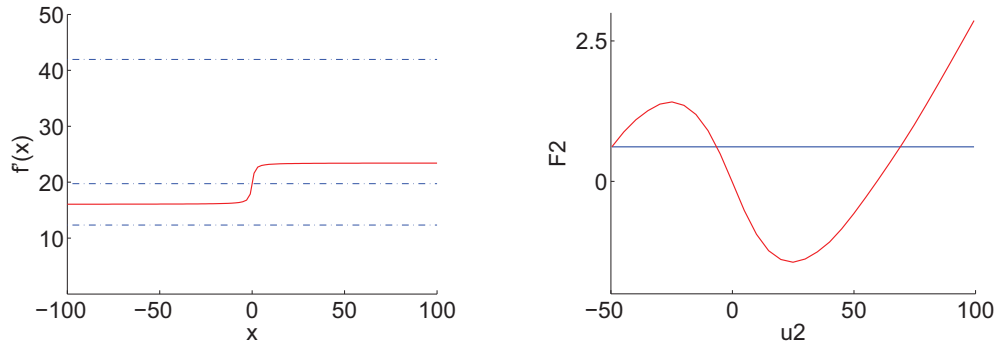**The Case J $= \{2\}$, for both Convex and Non-convex f**

Figure 5.11: $\overline{\operatorname{Ran} f'} \cap \sigma(-\Delta) = \{\lambda_2\}$

For an example of a convex f interacting with λ_2, we take $f'(x) = \alpha \arctan(x) + \beta$ so that $\operatorname{Ran} f' = \left(\lambda_2 - \frac{\lambda_2 - \lambda_1}{2}, \lambda_2 + \frac{\lambda_2 - \lambda_1}{2}\right)$. We have now *three* preimages $\beta_1 = -50\,\varphi_2 + 10\,\varphi_1$, β_2 and β_3 in the fiber. Again, $g = F(\beta_1)$. Figure 5.11 shows the behavior of the projections along the fiber and Figure 5.12 the three solutions.
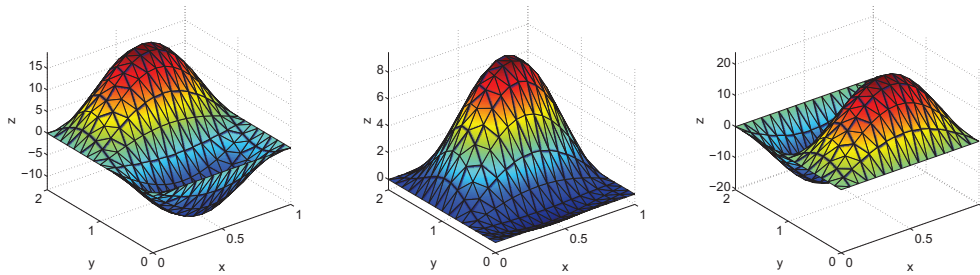

Figure 5.12: Convex Nonlinearity, $J = \{2\}$

In Figure 5.13 we exchange φ_1 and φ_2 and present a sequence similar to the one in Figure 5.10. This time, however, the action of F seems uniform
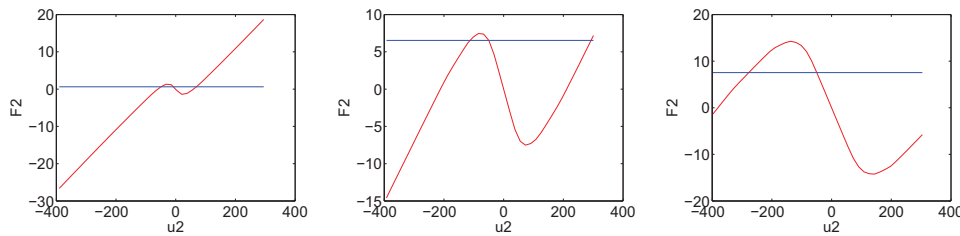

Figure 5.13: Fibers Getting Mapped Uniformly in Convex Case
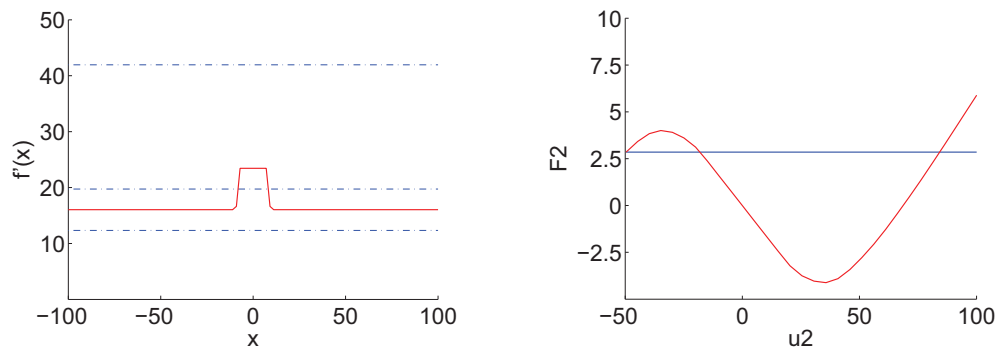
across fibers.

Figure 5.14: Non-convex f

We now consider a non-convex nonlinearity given in Figure 5.14. Things here are somewhat similar. There are again three solutions $\gamma_1 = \beta_1$, γ_2 and γ_3 for the right-hand $g = F(\gamma_1)$, shown in Figure 5.15. In this case, there is
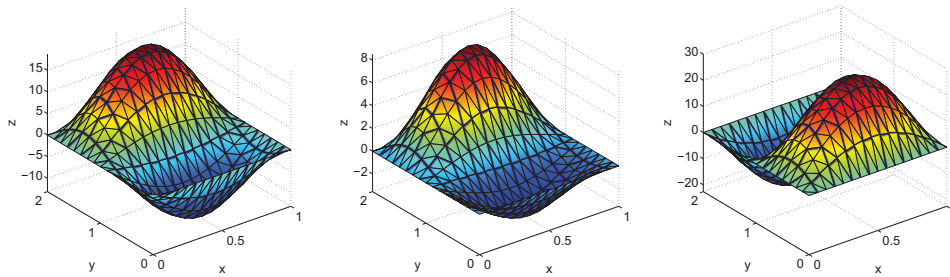

Figure 5.15: Solutions of non-convex case
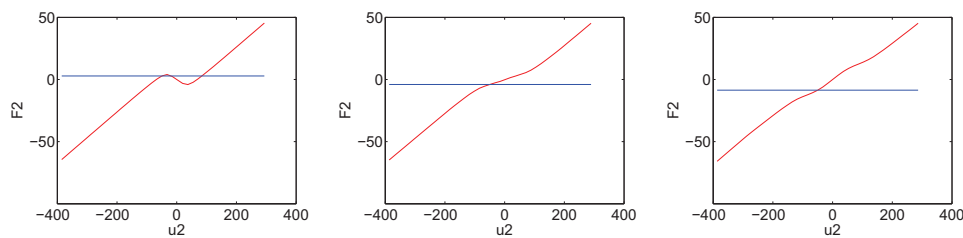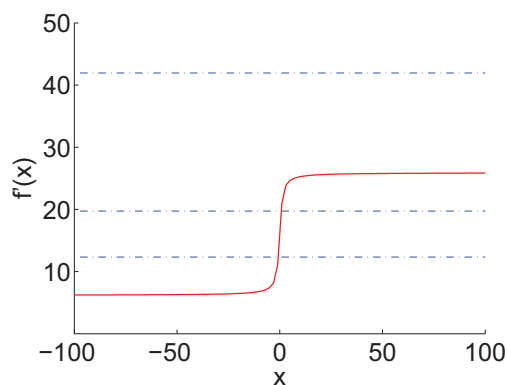
nonuniformity across fibers, as shown in Figure 5.16.

Figure 5.16: Non-Uniform Behavior Across Fibers

5.3
Interacting With Two Eigenvalues

In this concluding section, we attempt to picture the action of F on a two-dimensional fiber.

More specifically, we consider the fiber α_0 through the zero function, for which $F(0) = 0$. Consider the curve $C_\alpha \subset \alpha_0$ which projects bijectively

under Q_1 to the unit circle C in the vertical plane spanned by the first two eigenfunctions φ_1 and φ_2. Notice that, given a point in C, one may identify the corresponding point in C_α by moving horizontally with the first step of the algorithm.
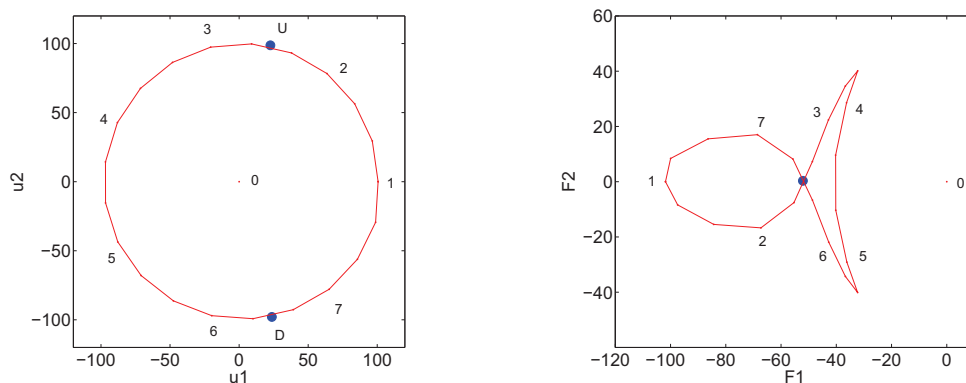

Figure 5.17: Solutions U and D on the circle C and images.

Next, we compute $F(C_\alpha)$, and project it by Q_{-1} to the vertical plane in the image. The result is the fish-shaped curve on the right of Figure 5.17. Notice that seven points were labeled, to indicate their positions in the domain and their image, giving an idea of how the curve is being traversed.

In particular, it is clear that there should be points U and V between points 2 and 3 and 6 and 7, respectively, with a common image g marked with a bullet on the right of Figure 5.17. Notice also that the origin is taken to outside of $F(C_\alpha)$, to its right.

Now radial lines in the domain from the origin to points in C give rise to lines from $F(0) = 0$ to points in $F(C_\alpha)$, as in 5.18. From this picture, we were able to obtain two additional approximations L and R along the horizontal axis for preimages of g.

The four approximate preimages were then taken as initial guesses for Newton's Method and the four computed solutions are illustrated in Figure 5.19.
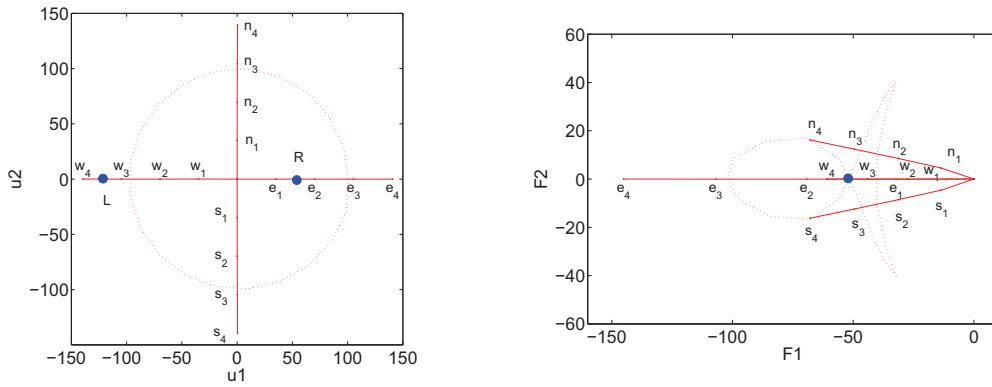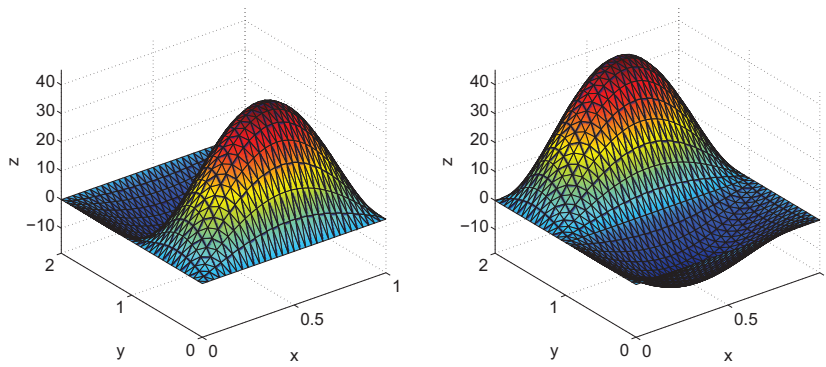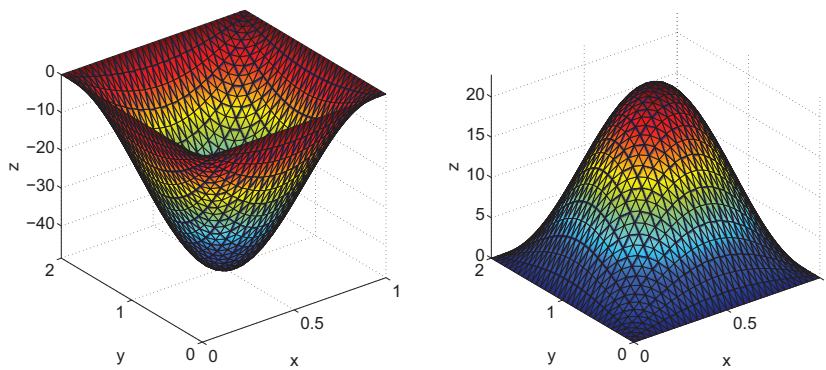

Figure 5.18: Solutions L and R on the u1 axis

5.19(a): U and D

5.19(b): L and R

Figure 5.19: Computed Solutions, 2-D case